

A Single-Phase Grid-Connected Fuel Cell System Based on a Boost-Inverter

Minsoo Jang, *Student Member, IEEE*, Mihai Ciobotaru, *Member, IEEE*,
and Vassilios G. Agelidis, *Senior Member, IEEE*

Abstract—In this paper, the boost-inverter topology is used as a building block for a single-phase grid-connected fuel cell (FC) system offering low cost and compactness. In addition, the proposed system incorporates battery-based energy storage and a dc–dc bidirectional converter to support the slow dynamics of the FC. The single-phase boost inverter is voltage-mode controlled and the dc–dc bidirectional converter is current-mode controlled. The low-frequency current ripple is supplied by the battery which minimizes the effects of such ripple being drawn directly from the FC itself. Moreover, this system can operate either in a grid-connected or stand-alone mode. In the grid-connected mode, the boost inverter is able to control the active (P) and reactive (Q) powers using an algorithm based on a second-order generalized integrator which provides a fast signal conditioning for single-phase systems. Design guidelines, simulation, and experimental results taken from a laboratory prototype are presented to confirm the performance of the proposed system.

Index Terms—Boost inverter, fuel cell, grid-connected inverter, power conditioning system (PCS), PQ control.

I. INTRODUCTION

ALTERNATIVE energy generation systems based on solar photovoltaics and fuel cells (FCs) need to be conditioned for both dc and ac loads. The overall system includes power electronics energy conversion technologies and may include energy storage based on the target application. However, the FC systems must be supported through additional energy storage unit to achieve high-quality supply of power [1]–[4]. When such systems are used to power ac loads or to be connected with the electricity grid, an inversion stage is also required.

The typical output voltage of low-power FC is low and variable with respect to the load current. For instance, based on the current–voltage characteristics of a 72-cell proton exchange membrane FC (PEMFC) power module, the voltage varies between 39 and 69 V depending upon the level of the output current as shown in Fig. 1 [5]. Moreover, the hydrogen and oxidant cannot respond the load current changes instantaneously due to the operation of components such as pumps, heat exchangers, and fuel-processing unit [6]–[8]. Caisheng *et al.* [9]

presented the cold-start which takes more than few seconds. Thus, the slow dynamics of the FC must be taken into account when designing FC systems. This is crucial, especially when the power drawn from the FC exceeds the maximum permissible power, as in this case, the FC module may not only fail to supply the required power to the load but also cease to operate or be damaged [10]–[12]. Therefore, the power converter needs to ensure that the required power remains within the maximum limit [10], [12].

A two-stage FC power conditioning system to deliver ac power has been commonly considered and studied in numerous technical papers [3], [4], [7], [10]–[14]. The two-stage FC power conditioning system encounters drawbacks such as being bulky, costly, and relatively inefficient due to its cascaded power conversion stages.

To alleviate these drawbacks, a topology that is suitable for ac loads and is powered from dc sources able to boost and invert the voltage at the same time has been proposed in [15]. The double loop control scheme of this topology has also been proposed for better performance even during transient conditions [16].

A single-stage FC system based on a boost inverter has been proposed in [17]. The single-stage system is able to minimize the problems with the two-stage FC power conditioning system [17]. The paper reported overall efficiency dealing with the single-stage and conventional two-stage FC systems. The total efficiency of the single-stage system has been improved around 10% over the range of the power rating and [17]. The paper illustrated the performance of a stand-alone FC system using the boost inverter with a bidirectional backup storage unit to support the slow dynamics of the FC and to cancel the ripple current that causes reduction of the lifetime and efficiency of the FC [17]–[19]. However, the performance and operating characteristics of such a system for grid applications is an important step forward that is yet to be reported in the technical literature.

The objective of this paper is to propose and report full experimental results of a grid-connected single-phase FC system using a single energy conversion stage only. In particular, the proposed system, based on the boost inverter with a backup energy storage unit, solves the previously mentioned issues (e.g., the low and variable output voltage of the FC, its slow dynamics, and current harmonics on the FC side). The single energy conversion stage includes both boosting and inversion functions and provides high power conversion efficiency, reduced converter size, and low cost [17]. The proposed single-phase grid-connected FC system can operate either in grid-connected or stand-alone mode. In the grid-connected mode, the boost-inverter is able to control the active (P) and reactive (Q) powers

Manuscript received December 20, 2011; revised March 1, 2012 and April 30, 2012; accepted April 30, 2012. Date of current version September 11, 2012. This paper was presented in part at the 2011 IEEE 8th International Conference on Power Electronics, Jeju, Korea, June 2011. Recommended for publication by Associate Editor S. Choi.

The authors are with the School of Electrical Engineering and Telecommunications, The University of New South Wales, Sydney, N.S.W. 2052, Australia (e-mail: minsoo@ieee.org; mihai.ciobotaru@unsw.edu.au; vassilios.agelidis@unsw.edu.au).

Color versions of one or more of the figures in this paper are available online at <http://ieeexplore.ieee.org>.

Digital Object Identifier 10.1109/TPEL.2012.2199770

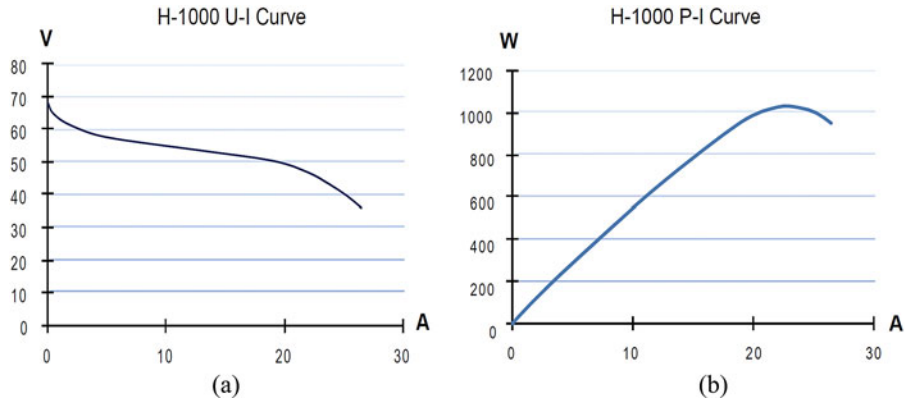


Fig. 1. Seventy-two-cell PEMFC system (Horizon H-1000, 1.0 kW). (a) Voltage–current characteristic showing the dc output voltage ranges from 39 to 69 V across the operating range. At rated power, dc output voltage and current are 43 and 23.5 A, respectively. (b) Power–current characteristic showing the output power ranges from zero when being idle to 1000 W at rated output power.

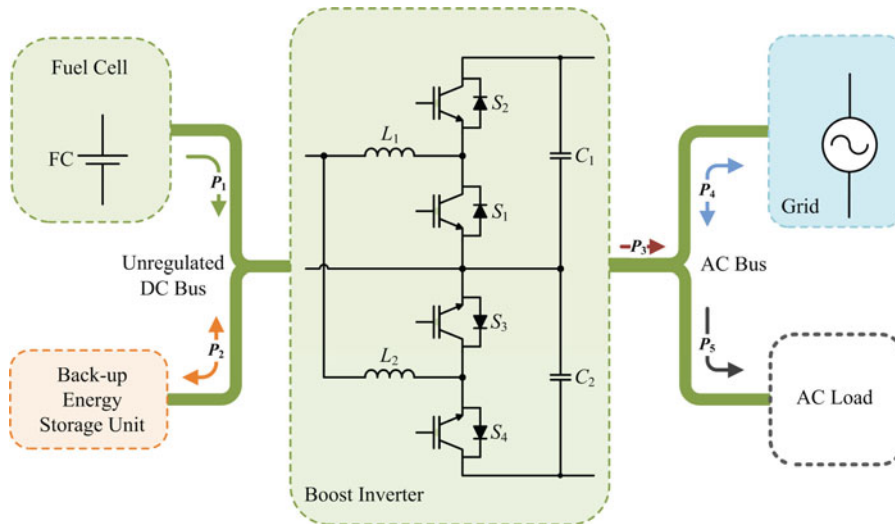


Fig. 2. Block diagram for the proposed grid-connected FC system. The backup unit and the FC power module are connected in the unregulated dc bus and the boost-inverter output is connected to the local load and the grid. (P1: FC output power, P2: backup unit input/output power, P3: inverter output power, P4: power between the inverter and the grid, and P5: power to the ac loads).

through the grid by the proposed PQ control algorithm using fast signal conditioning for single-phase systems [20].

The remaining of this paper is organized as follows. In Section II, the proposed grid-connected FC system is introduced including the inverter topology, the control algorithm of the boost inverter, the backup energy storage unit, and the PQ control algorithm for a single-phase FC system. Design guidelines are also provided in Section II. In Section III, simulation and experimental results are presented to document the performance of the proposed system. Experimental results taken from a 1-kW laboratory prototype are presented to verify the overall performance of the proposed grid-connected FC system. Finally, the conclusions are summarized in Section IV.

II. PROPOSED FC ENERGY SYSTEM

A. Description of the FC System

The block diagram of the proposed grid-connected FC system is shown in Fig. 2. Fig. 2 also shows the power flows between

each part. This system consists of two power converters: the boost inverter and the bidirectional backup unit, as shown in Figs. 2 and 3. Fig. 4 shows the laboratory setup of the proposed FC system. The boost inverter is supplied by the FC and the backup unit, which are both connected to the same unregulated dc bus, while the output side is connected to the load and grid through an inductor. The system incorporates a current-mode controlled bidirectional converter with battery energy storage to support the FC power generation and a voltage-controlled boost inverter.

The FC system should dynamically adjust to varying input voltage while maintaining constant power operation. Voltage and current limits, which should be provided by the manufacturers of the FC stack, need to be imposed at the input of the converter to protect the FC from damage due to excessive loading and transients. Moreover, the power has to be ramped up and down so that the FC can react appropriately, avoiding transients and extending its lifetime. The converter also has to meet the maximum ripple current requirements of the FC [6].

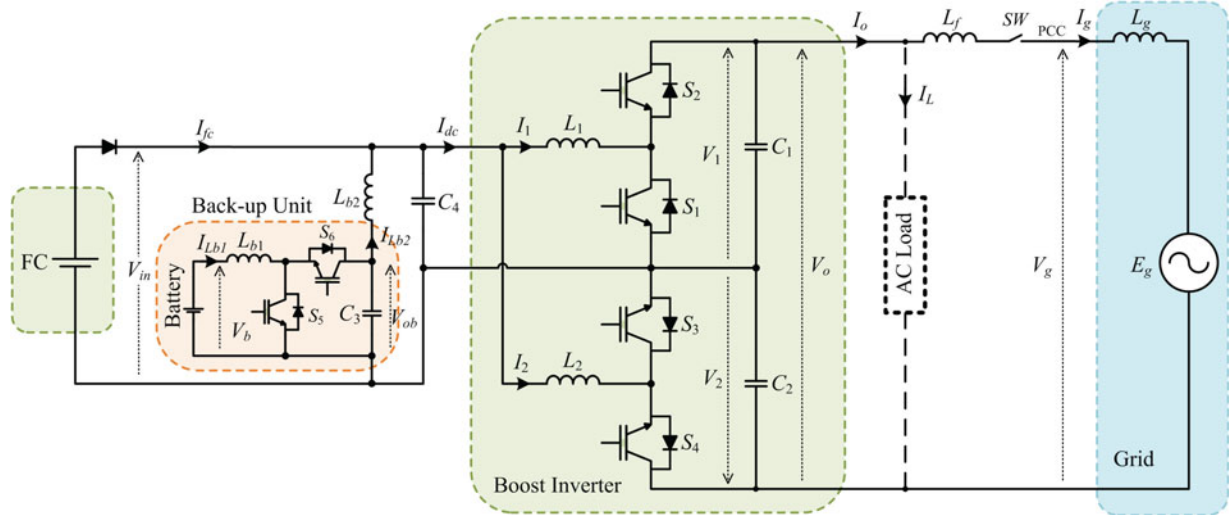


Fig. 3. General structure of the proposed grid-connected FC system.

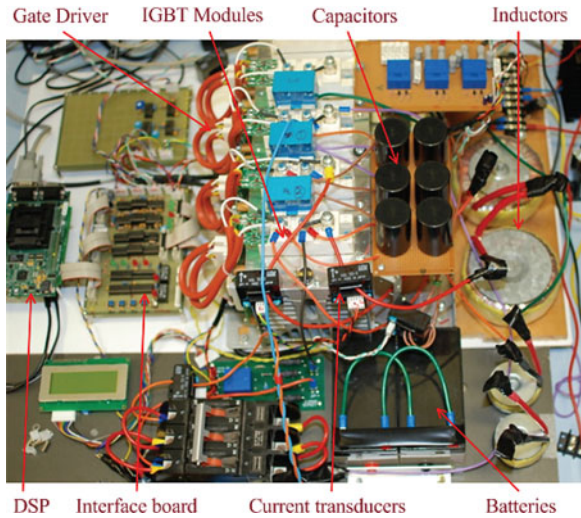


Fig. 4. Laboratory prototype of the proposed grid-connected FC system.

In the grid-connected mode, the system is also providing active (P) and reactive (Q) power control. A key concept of the PQ control in the inductive coupled voltage sources is the use of a grid compatible frequency and voltage droops [20]. Therefore, the active and reactive powers are controlled by the small variations of the voltage phase and magnitude. The control of the inverter requires a fast signal conditioning for single-phase systems. In the proposed system, the second-order generalized integrator (SOGI) algorithm has been employed [20].

B. Boost Inverter

The boost inverter consists of two bidirectional boost converters and their outputs are connected in series, as shown in Fig. 3. Each boost converter generates a dc bias with deliberate ac output voltage (a dc-biased sinusoidal waveform as an output), so that each converter generates a unipolar voltage greater than the FC voltage with a variable duty cycle. Each converter

output and the combined outputs are described by

$$V_1 = V_{dc} + 1/2 \cdot A_1 \cdot \sin \theta \quad (1)$$

$$V_2 = V_{dc} + 1/2 \cdot A_2 \cdot \sin(\theta - \pi) \quad (2)$$

$$V_o = V_1 - V_2 = A_o \cdot \sin \theta, \text{ when } A_o = A_1 = A_2 \quad (3)$$

$$V_{dc} > V_{in} + \frac{A_o}{2} \quad (4)$$

where V_{dc} is the dc offset voltage of each boost converter and have to be greater than $0.5 A_o + V_{in}$.

From (3), it can be observed that the output voltage V_o contains only the ac component. This concept has been discussed in numerous papers [15], [16]. The boost inverter employs voltage-mode control.

In this paper, a double-loop control scheme is chosen for the boost-inverter control being the most appropriate method to control the individual boost converters covering the wide range of operating points. This control method is based on the averaged continuous-time model of the boost topology and has several advantages with special conditions that may not be provided by the sliding mode control, such as nonlinear loads, abrupt load variations, and transient short-circuit situations. Using this control method, the inverter maintains a stable operating condition by means of limiting the inductor current. Because of this ability to keep the system under control even in these situations, the inverter achieves a very reliable operation [16].

The reference voltage of the boost inverter is provided from the PQ control algorithm being able to control the active and reactive power. The voltages across C_1 and C_2 are controlled to track the voltage references using proportional-resonant (PR) controllers. Compared with the conventional proportional-integral (PI) controller, the PR controller has the ability to minimize the drawbacks of the PI one such as lack of tracking a sinusoidal reference with zero steady-state error and poor disturbance rejection capability [21], [22].

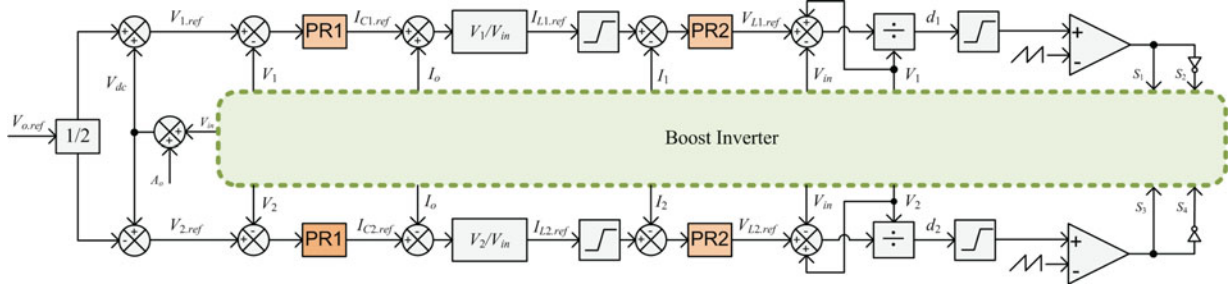


Fig. 5. Boost-inverter control block diagram.

The currents through L_1 and L_2 are controlled by PR controllers to achieve a stable operation under special conditions such as nonlinear loads and transients.

The control block diagram for the boost inverter is shown in Fig. 5. The output voltage reference is divided to generate the two individual output voltage references of the two boost converters with the dc bias, V_{dc} . The dc bias can be obtained by adding the input voltage V_{in} to the half of the peak output amplitude. V_{dc} is also used to minimize the output voltages of the converters and the switching losses in the variable input voltage condition.

The output voltage reference is determined by

$$V_{o.ref} = (V_{pp} + dV_{pp}) \cdot \sin(\omega_o t + \delta), \quad \text{when} \\ A_o = V_{pp} + dV_{pp} \quad \text{and} \quad \theta = \omega_o t + \delta \quad (5)$$

where V_{pp} is the peak value of the typical grid voltage, dV_{pp} is a small variation of the output voltage reference affecting to the reactive power, ω_o is the grid fundamental angular frequency, and δ is the phase difference between V_o and V_g relating with the active power. Then, $V_{1.ref}$ and $V_{2.ref}$ are calculated by (1) and (2).

C. Backup Energy Storage Unit

The functions of the backup energy storage unit are divided into two parts. First, the backup unit is designed to support the slow dynamics of the FC. Second, in order to protect the FC system, the backup unit provides low-frequency ac current that is required from the boost inverter operation. The low-frequency current ripple supplied by the batteries has an impact on their lifetime [23], but between the most expensive FC components and the relatively inexpensive battery components, the latter is preferable to be stressed by such low-frequency current ripple. The backup unit comprises of a current-mode controlled bidirectional converter and a battery as the energy storage unit. For instance, when a 1-kW load is connected from a no-load condition, the backup unit immediately provides the 1-kW power from the battery to the load, as shown in Table I. On the other hand, when the load is disconnected suddenly, the surplus power from the FC could be recovered and stored into the battery to increase the overall efficiency of the energy system.

The backup unit controller is designed to control the output current of the backup unit in Fig. 6. The reference of I_{Lb1} is determined by I_{dc} through a high-pass filter and the demanded current I_{demand} that is related to the load change. The ac

TABLE I
BACKUP UNIT SEQUENCE OF MODES OF OPERATION UNDER LOAD CHANGE

P_3 Increase ($P_1+P_2 \rightarrow P_3$)	P_3 Decrease ($P_1 \rightarrow P_2+P_3$)	Normal ($P_1=P_3$)
Discharge		
↓		
Charge	Charge	
↓	↓	
Normal	Normal	Normal

component of the current reference deals with eliminating the ac ripple current into the FC power module while the dc component deals with the slow dynamics of the FC.

D. Control of the Grid-Connected Boost Inverter

Fig. 7 illustrates the equivalent circuit of the grid-connected FC system consisting of two ac sources (V_g and V_o), an ac inductor L_f between the two ac sources, and the load. The boost inverter output voltage (including the FC and backup unit) is indicated as V_o and V_g is the grid voltage. The active and reactive powers at the point of common coupling (PCC) are expressed by [20] and [24]

$$P = \frac{V_g \cdot V_o}{\omega_o \cdot L_f} \sin(\delta) \quad (6)$$

$$Q = \frac{V_g^2}{\omega_o \cdot L_f} - \frac{V_g \cdot V_o}{\omega_o \cdot L_f} \cos(\delta) \quad (7)$$

where L_f is the filter inductance between the grid and the boost inverter.

From (6) and (7), the phase shift δ and voltage difference $V_g - V_o$ between V_o and V_g affect the active and the reactive powers, respectively. Therefore, to control the power flows between the boost inverter and the grid, the FC system must be able to vary its output voltage V_o in amplitude and phase with respect to the grid voltage V_g [20], [24].

Fig. 8 shows the theoretical approach to control the power between the grid and the boost inverter with different vector diagrams. According to these vector diagrams, power flow, active power and reactive powers should be controlled by the phase angle δ and the inverter voltage amplitude, V_o . For instance, when the reactive power reference is zero, Fig. 8(a) shows active power controlling with small variations of δ and dV_{pp} . If active and reactive powers need to be controlled simultaneously, Fig. 8(b) is the approach to control them. Fig. 8(c) illustrates

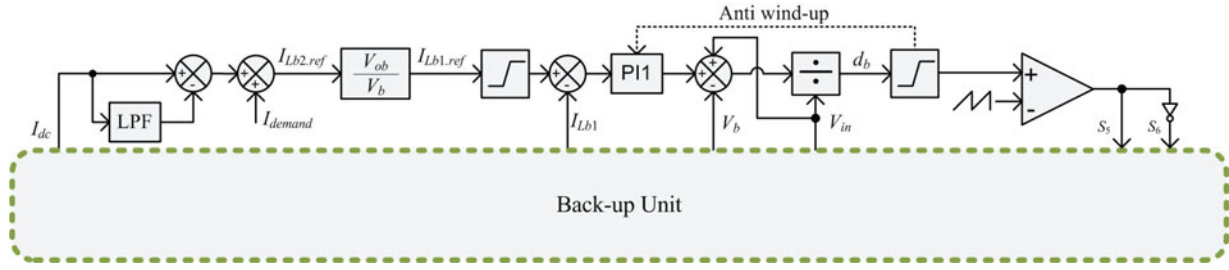


Fig. 6. Backup unit control block diagram.

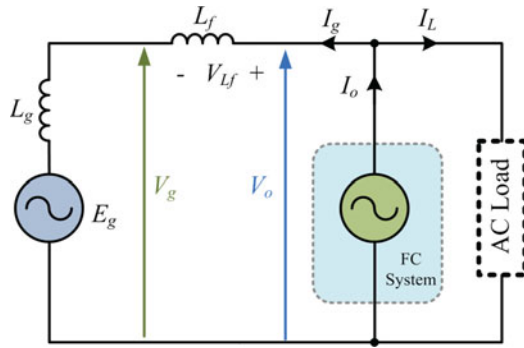


Fig. 7. Equivalent circuit of the grid-connected FC system.

that only dV_{pp} is controlled for reactive power while the active power is zero by the magnitude of V_o equals V_g .

Fig. 8 illustrates that the system is sensitive to small changes of the phase δ and the magnitude dV_{pp} . Therefore, the grid-connected FC system as parallel operation of voltage source inverters requires a precise control. Grid-compatible frequency and voltage droop were introduced to control active and reactive powers in this paper. The droop control for the boost inverter requires the fast acquisition of P and Q . The measurement of P and Q at the PCC is obtained based on the following expressions [20]:

$$P_{meas} = \frac{1}{2}(v_{g\alpha} \cdot i_{g\alpha} + v_{g\beta} \cdot i_{g\beta}) \quad (8)$$

$$Q_{meas} = \frac{1}{2}(v_{g\beta} \cdot i_{g\alpha} - v_{g\alpha} \cdot i_{g\beta}) \quad (9)$$

where $v_{g\alpha}$ and $v_{g\beta}$ are the instantaneous orthogonal voltages at PCC, and $i_{g\alpha}$ and $i_{g\beta}$ are the instantaneous orthogonal currents at PCC. The orthogonal voltage and current are obtained using a SOGI-based algorithm which provides a fast signal conditioning for single-phase systems [20].

Fig. 9 illustrates the PQ control algorithm with the phase-locked loop and the orthogonal system generator. δ and dV_{pp} are determined by PI regulators to track the active and reactive power references. The inverter voltage reference is generated to control the active and reactive powers using the droop control method, as shown in Fig. 9.

E. Design Guidelines

The power components of the proposed system were designed with the parameters given in Table II.

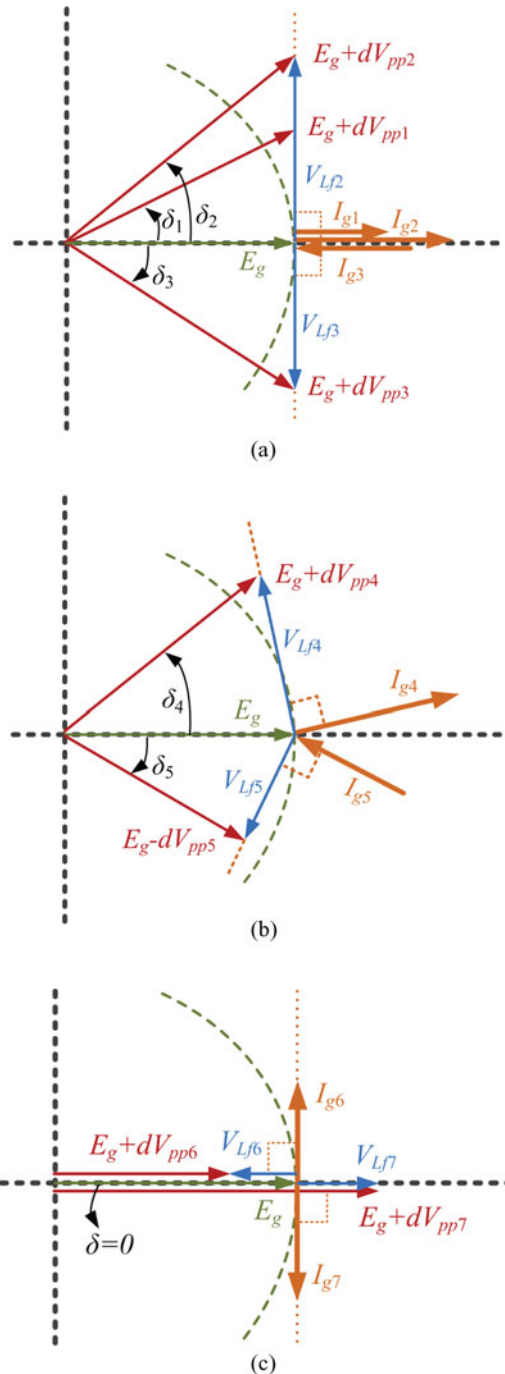


Fig. 8. Vector diagrams for the active and reactive power control. (a) When reactive power reference is zero. (b) Active and reactive powers are controlled simultaneously. (c) When active power reference is zero.

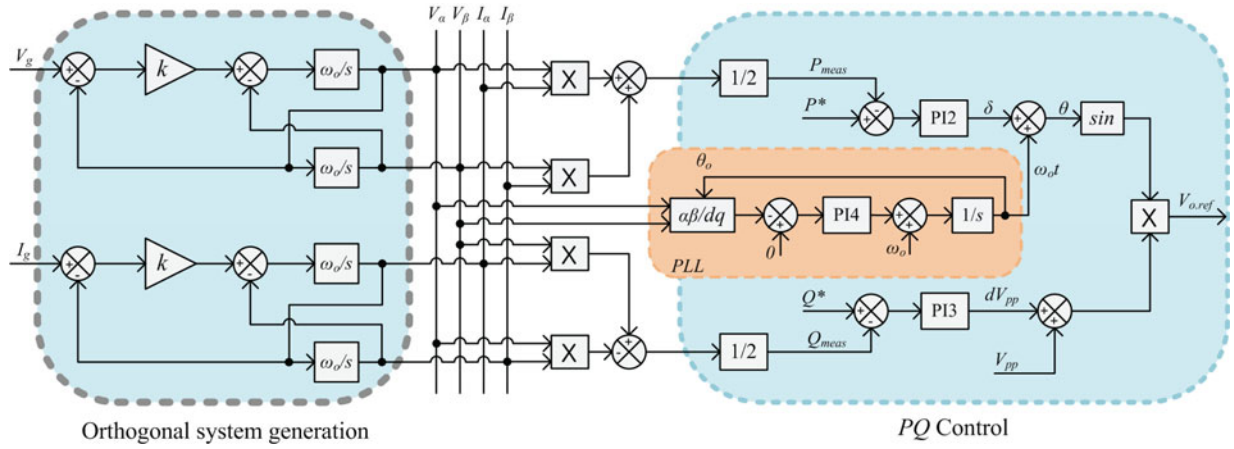


Fig. 9. Boost-inverter output voltage reference generation block diagram with the PQ control algorithm.

TABLE II
DESIGN SPECIFICATIONS

FC output voltage	36-69V (72-Cell FC)
AC output voltage	220V RMS, Single phase, 50Hz
AC Grid voltage	220V, 50Hz
Switching frequency	20kHz
Output power	1kW
V_{in}	42V (min)
R_a (resistance of L_1 and L_2)	$\approx 10m\Omega$
$V_1(t)$	353V (max)
$V_2(t)$	42V (min)
Δt_f (maximum on time)	42.5 μ s (max at 20kHz)
Δi_{Lmax}	5% of $i_{L(max)}$
ΔV_c	5% of V_{1max}
R_1 (load)	48.4 Ω at 1kW
V_b (battery voltage)	22V(min)-27.3V(max)
I_{Lb1}	45.5A (max)

TABLE III
SPECIFICATIONS FOR THE FC SYSTEM

FC output voltage	39-69V (72 Cell PEMFC)
AC output voltage	220V, 50Hz
Switching frequency	20kHz
Rated power	1.0kW (43V at 23.5A)
Power stack	SEMISTACK-IGBT
Controller	DSP TMS320F28335
Voltage transducers	LEM LV25-P
Current transducers	LEM HAL50s
Energy storage	Two 12V-24Ah lead acid batteries
$L_1=L_2$	700 μ H
$L_{b1}=L_{b2}$	150 μ H
L_f	5mH
$C_1=C_2=C_3=C_4$	20 μ F
$PR1$	$K_P:0.1, K_I:10$
$PR2$	$K_P:1, K_I:1000$
$PI1$	$K_P:0.1, K_I:100$
$PI2$	$K_P:1e-6, K_I:1e-3$
$PI3$	$K_P:5e-5, K_I:0.2$
$PI4$	$K_P:0.5, K_I:0.03$

The current of the inductors (i_{L1} , i_{L2}) consists of fundamental and switching frequency components. To calculate the inductance of L_1 and L_2 , the following equations are used [15]:

$$i_L(\max) = \frac{V_{in} - \sqrt{V_{in}^2 - 4R_a(-V_1(t)) \cdot ((V_2(t) - V_1(t))/R_1)}}{2R_a} \quad (10)$$

$$\Delta i_L(t) = \frac{(V_{in} - R_a i_L(t)) \cdot \Delta t_1}{L} \quad (11)$$

where $i_L(\max)$ is maximum inductor current and Δi_L is high-frequency ripple current of the inductor caused by switching. The maximum inductor current ripple Δi_{Lmax} is chosen to be equal to 5% of the maximum inductor current, as calculated from (10) when the V_1 is maximum and V_2 is minimum. From (10) and (11), the minimum inductance is calculated as 650 and 700 μ H which are the chosen values for L_1 and L_2 . The ripple

voltage of the C_1 and C_2 is given by [15]

$$\Delta V_c = \left(\frac{V_1(t) - V_2(t)}{C \cdot R_1} \right) \cdot \Delta t_1. \quad (12)$$

A 15- μ F designed capacitor value has been obtained using (12) and a 20- μ F 800-V rated metallized polypropylene film capacitor has been used as C_1 and C_2 for the experimental setup, as shown in Fig. 4. The same value of 20 μ F has been used for the backup unit capacitors C_3 and C_4 .

During transient conditions, the backup unit should provide all the power required by the load. In this case, the maximum inductor current of the boost inverter should appear in the inductor L_{b2} . Therefore, the maximum inductance of L_{b2} can be

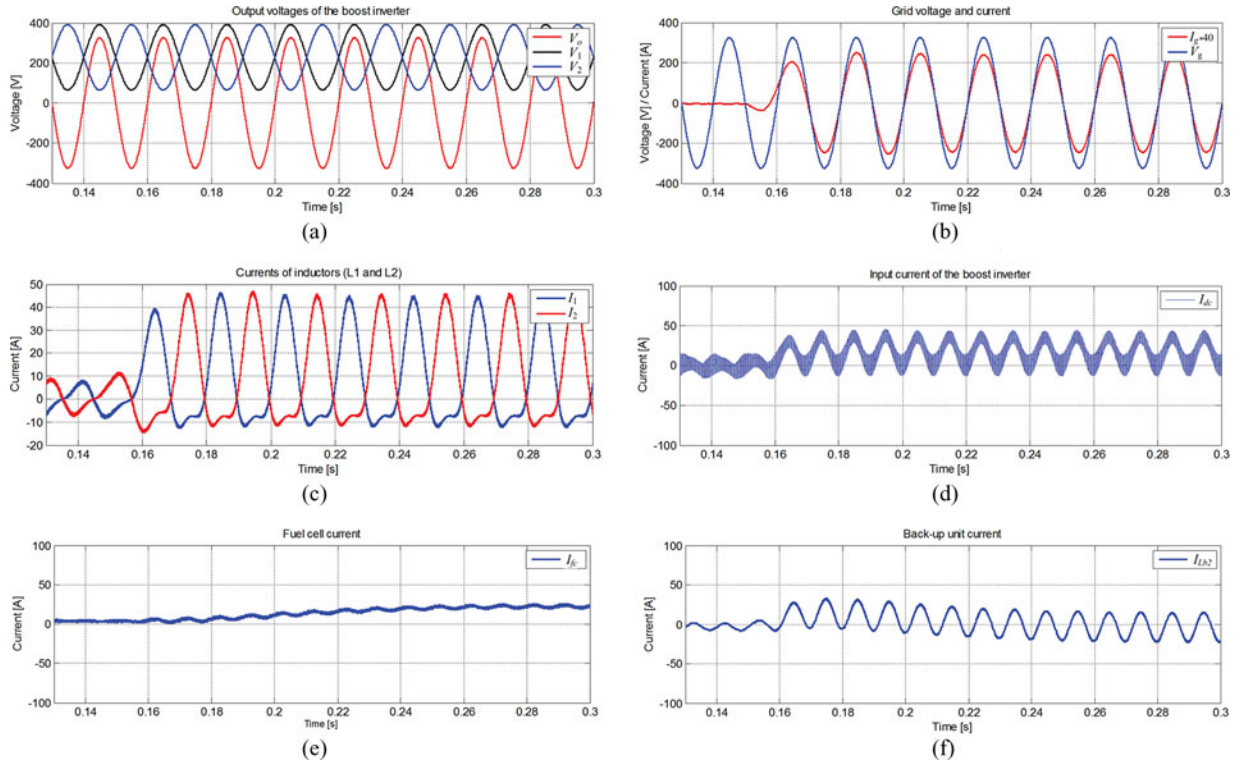


Fig. 10. Simulation results of the proposed FC system. (a) Output voltages of the boost inverter. (b) Grid voltage V_g and current I_g with full power feeding to the grid. (c) Current waveforms of L_1 and L_2 . (d) Input current of the boost inverter, I_{dc} . (e) FC output current during transient, I_{fc} . (f) Output current of the backup unit, I_{Lb2} .

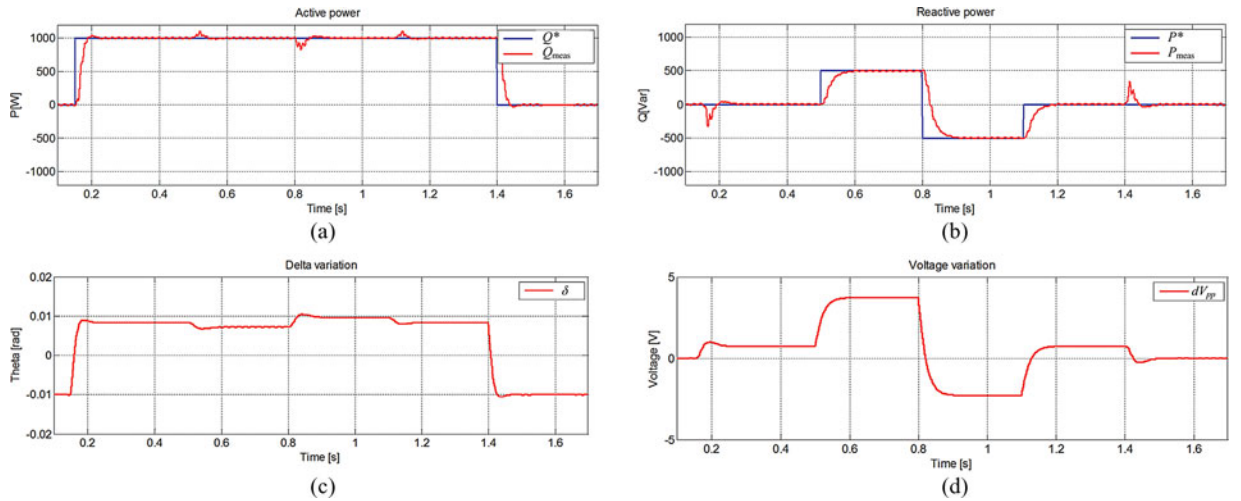


Fig. 11. Simulation results of the PQ control. (a) Active power measurement and its reference. (b) Reactive power measurement and its reference. (c) Small variation of the phase δ for the active power control. (d) Small variation of the voltage amplitude dV_{pp} for the reactive power control.

calculated by (11) and $\Delta I_L(t)_{max}$ need to be larger than the maximum inductor current of the boost inverter in order to track the maximum slope of the current. The maximum inductance is obtained from (11) as $366 \mu\text{H}$ and the values of L_{b1} and L_{b2} are chosen to be $150 \mu\text{H}$.

The capacity of the battery should be designed to recover the slow dynamics (maximum current slew rate is 4 A/s [12]) and start up time (30 s at room temperature [5]) of the FC. Two generic 12-V lead-acid batteries are introduced for energy

storage to deal with the need to provide fast dynamics and a relatively low-cost solution. The FC startup time should be considered as worst case scenario to calculate the battery capacity. The minimum and maximum voltages of the battery are shown in Table II. The battery consists of six cells and recommended float voltage for the batteries at 25°C is 2.26 V/cell and the capacity choice guideline is provided in the battery’s manual [25]. To find the minimum voltage per cells, the minimum voltage of the battery is divided by the number of cells ($22/12 = 1.833 \text{ V/cell}$).

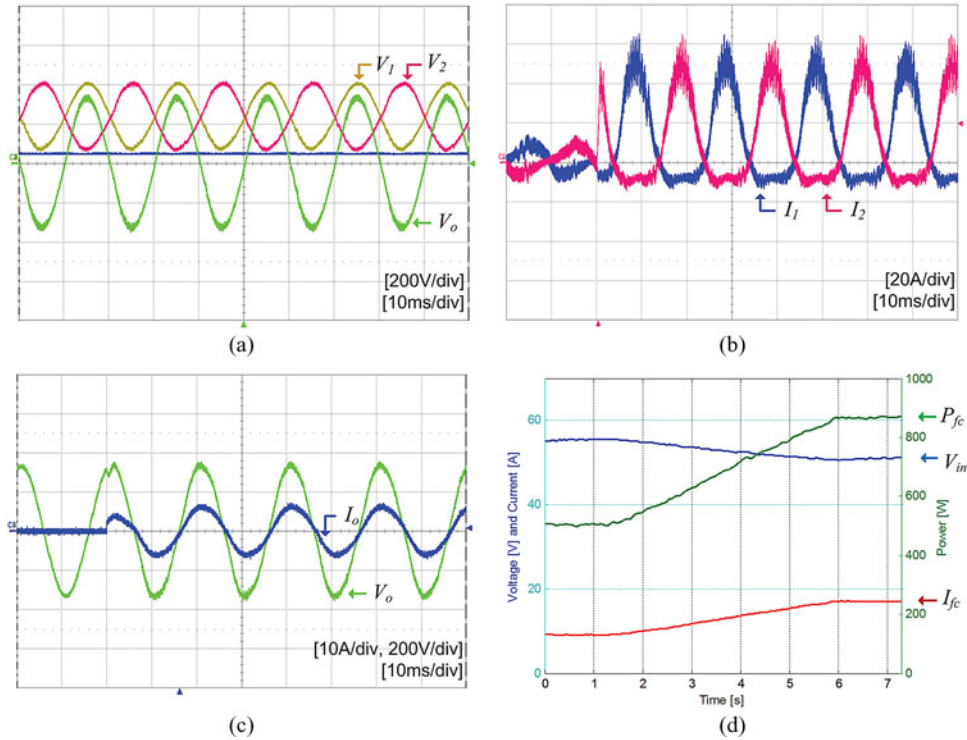


Fig. 12. Experimental results. (a) Output voltages of the boost inverter (V_1 , V_2 , and V_o) and dc input voltage, V_{in} . (b) Current waveforms of L_1 and L_2 . (c) Voltage and current of the boost inverter when full-load is connected, V_o and I_o . (d) When the load is increased, the backup unit supports the ramp-up operation for the FC.

The load Watts per cell is obtained as the rated power divided by the number of cells ($1000/12 = 83.33$ W/cell). The value of Watts per cell per Ah can be found at 4.13 in the provided Watts/Ah/Cell table [25]. The minimum battery capacity is obtained as the load Watts per cell divided by the value from the Watts/Ah/Cell table ($83.33/4.13 = 20$ Ah). Therefore, a 24-Ah battery is selected for the system.

III. SIMULATION AND EXPERIMENTAL RESULTS

The proposed FC system (see Fig. 3) has been analyzed, designed, simulated, and tested experimentally to validate its overall performance. The simulations have been done using Simulink/MATLAB and PLECS blockset to validate the analytical results. The ac output voltage of the system was chosen to be equal to 220 V, while the dc input voltage varied between 43 and 69 V. The parameters of the proposed FC system for the simulation and the laboratory prototype (see Fig. 4) are summarized in Table III.

The simulation results show the operations of the boost inverter and the backup unit. In particular, Fig. 10(a) illustrates the output voltages of the boost inverter (V_1 , V_2 , and V_o) and Fig. 10(b) shows the grid voltage and grid current at the PCC. The input currents of each boost converter flowing through the inductors L_1 and L_2 are shown in Fig. 10(c). Fig. 10(d)–(f) illustrates the waveforms of the inverter input current I_{dc} , the FC output current I_{fc} , and the output current I_{Lb2} of the backup unit, respectively. Fig. 10(e) and (f) also illustrates how the backup unit supports the FC power in transients when the load is in-

creased at 0.15 s. When full-load is required from the no-load operating point, the entire power is provided by the backup unit to the load, as shown in Fig. 10(f). Then, the power drawn from the battery starts decreasing moderately allowing gentle step-up to deliver power which should increase up to meet the demanded load power. Moreover, the backup unit protects the FC from potential damage by eliminating the ripple current due to the boost operation. The high-frequency output ripple current of the FC can be canceled by a passive filter placed between the FC and the boost inverter. The active and reactive power control performances are illustrated with the references and the measured values in Fig. 11(a) and (b). In addition, Fig. 11(c) and (d) shows the variation of the phase shift δ between V_o and V_g to control the active power and the variation of the voltage differences, $V_g - V_o$, related with the reactive power control, respectively.

The obtained experimental efficiency for the proposed system is about 93% at peak point and 83% at rated output power. Consequently, the proposed FC system achieves an increased total efficiency when compared with a conventional two-stage FC system [17].

The proposed single-phase grid-connected FC system has been developed as a laboratory prototype (see Fig. 4). In this paper, a dc power supply is used to provide dc output between 43 and 69 V, same voltage range as a 72-cell PEMFC. The power electronic stack consists of three insulated gate bipolar transistor (IGBT) modules that are used to build the boost inverter for two modules and backup unit for one module. The DSP controller unit has been used for a number of reasons such as low cost,

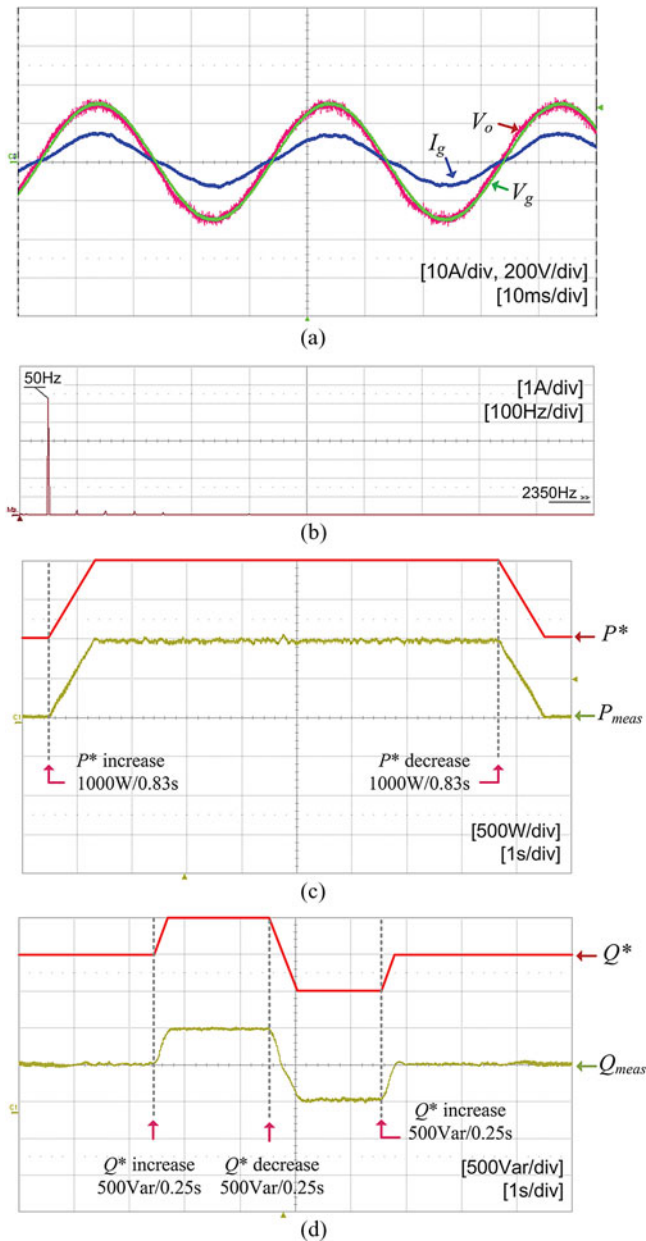


Fig. 13. Experimental results for the grid connection. (a) Inverter output voltage V_o , grid voltage V_g , and current through the inductor L_f (I_g) at 1-kW injection to the grid. (b) FFT of the grid current I_g . (c) Measured active power controlled between 0 and 1 kW. (d) Measured reactive power controlled between 500 and -500 Var.

embedded floating point unit, high speed, on-chip analog-to-digital converter, and high-performance pulsewidth modulation unit.

Experimental results presented in Fig. 12 show the performance of the boost inverter operation with the load changing. Specifically, Fig. 12(a) illustrates the input and output voltages of the boost inverter. The current waveforms of the two different inductors are shown in Fig. 12(b). The FC system output voltage and current are shown in Fig. 12(c). As can be seen in Fig. 12(d), the FC power changed from approximately 500 to 850 W in 5 s which is a moderate amount of time. Fig. 12(d) also illustrates

how the backup unit supports the FC, since the FC is expected to have a slow power up operation.

Experimental results for the grid connection of the FC system are presented in Fig. 13. Fig. 13(a) illustrates the current through the inductor L_f and the voltages of grid and inverter output (V_g and V_o). The difference between the two voltages is not visible due to the small amount of the phase angle being under 0.01[rad]. Fig. 13(b) shows the fast Fourier transform (FFT) of the grid current I_g with the total harmonic distortion (THD) being approximately 4%. Fig. 13(c) and (d) shows the active and reactive power control performance.

IV. CONCLUSION

A single-phase single power stage grid-connected FC system based on the boost-inverter topology with a backup battery-based energy storage unit is proposed in this paper. The simulation results and selected laboratory tests verify the operation characteristics of the proposed FC system. In summary, the proposed FC system has a number of attractive features, such as single power conversion stage with high efficiency, simplified topology, low cost, and able to operate in stand-alone as well as in grid-connected mode. Moreover, in the grid-connected mode, the single-phase FC system is able to control the active and reactive powers by a PQ control algorithm based on SOGI which offers a fast signal conditioning for single-phase systems. However, it should be noted that the voltage-mode control adopted for the boost inverter may result in a distorted grid current (under given THD) if the grid voltage includes a harmonic component.

REFERENCES

- [1] S. B. Kjaer, J. K. Pedersen, and F. Blaabjerg, "A review of single-phase grid-connected inverters for photovoltaic modules," *IEEE Trans. Ind. Appl.*, vol. 41, no. 5, pp. 1292–1306, Sep./Oct. 2005.
- [2] S. B. Kjaer, "Design and control of an inverter for photovoltaic applications," Ph.D. dissertation, Inst. Energy Technol., Aalborg Univ., Aalborg, Denmark, 2005.
- [3] J.-S. Lai, "Power conditioning circuit topologies," *IEEE Ind. Electron. Mag.*, vol. 3, no. 2, pp. 24–34, Jun. 2009.
- [4] M. E. Schenck, J.-S. Lai, and K. Stanton, "Fuel cell and power conditioning system interactions," in *Proc. IEEE Appl. Power Electron. Conf. Expo.*, Mar. 2005, vol. 1, pp. 114–120.
- [5] Horizon Fuel Cell Technologies, H-Series PEMFC System User Guide (2010). [Online]. Available: <http://www.horizonfuelcell.com>
- [6] J. Anzicek and M. Thompson, "DC-DC boost converter design for Kettering University's GEM fuel cell vehicle," in *Proc. Electr. Insul. Conf. Electr. Manuf. Expo.*, 2005, pp. 307–316.
- [7] X. Yu, M. R. Starke, L. M. Tolbert, and B. Ozpineci, "Fuel cell power conditioning for electric power applications: A summary," *IET Electr. Power Appl.*, vol. 1, pp. 643–656, 2007.
- [8] K. Jin, X. Ruan, M. Yang, and M. Xu, "Power management for fuel-cell power system cold start," *IEEE Trans. Power Electron.*, vol. 24, no. 10, pp. 2391–2395, Oct. 2009.
- [9] W. Caisheng, M. H. Nehrir, and S. R. Shaw, "Dynamic models and model validation for PEM fuel cells using electrical circuits," *IEEE Trans. Energy Convers.*, vol. 20, no. 2, pp. 442–451, Jun. 2005.
- [10] M. W. Ellis, M. R. Von Spakovsky, and D. J. Nelson, "Fuel cell systems: Efficient, flexible energy conversion for the 21st century," *Proc. IEEE*, vol. 89, no. 12, pp. 1808–1818, Dec. 2001.
- [11] J. Lee, J. Jo, S. Choi, and S.-B. Han, "A 10-kW SOFC low-voltage battery hybrid power conditioning system for residential use," *IEEE Trans. Energy Convers.*, vol. 21, no. 2, pp. 575–585, Jun. 2006.
- [12] P. Thounthong, B. Davat, S. Rael, and P. Sethakul, "Fuel cell high-power applications," *IEEE Ind. Electron. Mag.*, vol. 3, no. 1, pp. 32–46, Mar. 2009.

- [13] P. Ching-Tsai and L. Ching-Ming, "A high-efficiency high step-up converter with low switch voltage stress for fuel-cell system applications," *IEEE Trans. Ind. Electron.*, vol. 57, no. 6, pp. 1998–2006, Jun. 2010.
- [14] A. Vazquez-Blanco, C. Aguilar-Castillo, F. Canales-Abarca, and J. Arau-Roffiel, "Two-stage and integrated fuel cell power conditioner: Performance comparison," in *Proc. IEEE Appl. Power Electron. Conf. Expo.*, Feb. 2009, pp. 452–458.
- [15] R. O. Caceres and I. Barbi, "A boost DC-AC converter: Analysis, design, and experimentation," *IEEE Trans. Power Electron.*, vol. 14, no. 1, pp. 134–141, Jan. 1999.
- [16] P. Sanchis, A. Ursaea, E. Gubia, and L. Marroyo, "Boost DC-AC inverter: A new control strategy," *IEEE Trans. Power Electron.*, vol. 20, no. 2, pp. 343–353, Mar. 2005.
- [17] M. Jang and V. G. Agelidis, "A minimum power-processing-stage fuel-cell energy system based on a boost-inverter with a bidirectional backup battery storage," *IEEE Trans. Power Electron.*, vol. 26, no. 5, pp. 1568–1577, May 2011.
- [18] J. I. Itoh and F. Hayashi, "Ripple current reduction of a fuel cell for a single-phase isolated converter using a DC active filter with a center tap," *IEEE Trans. Power Electron.*, vol. 25, no. 3, pp. 550–556, Mar. 2010.
- [19] R.-J. Wai and C.-Y. Lin, "Active low-frequency ripple control for clean-energy power-conditioning mechanism," *IEEE Trans. Ind. Electron.*, vol. 57, no. 11, pp. 3780–3792, Nov. 2010.
- [20] B. Burger and A. Engler, "Fast signal conditioning in single phase systems," presented at the Eur. Conf. Power Electron. Appl., Graz, Austria, 2001.
- [21] R. Teodorescu, F. Blaabjerg, M. Liserre, and P. C. Loh, "Proportional-resonant controllers and filters for grid-connected voltage-source converters," *IEEE Proc.—Electr. Power Appl.*, vol. 153, pp. 750–762, 2006.
- [22] H. Cha, T.-K. Vu, and J.-E. Kim, "Design and control of proportional-resonant controller based photovoltaic power conditioning system," in *Proc. IEEE Energy Convers. Congr. Expo.*, Sep. 2009, pp. 2198–2205.
- [23] A. Jossen, "Fundamentals of battery dynamics," *J. Power Sources*, vol. 154, pp. 530–538, Mar. 2006.
- [24] B. Bouneb, D. M. Grant, A. Cruden, and J. R. McDonald, "Grid connected inverter suitable for economic residential fuel cell operation," in *Proc. Eur. Conf. Power Electron. Appl.*, 2005, pp. 1–10.
- [25] *NP-Series Lead Acid Battery Manual*, (2007). [Online]. Available: <http://www.yuasa-battery.co.uk>



Minsoo Jang (S'09) received the B.S. and M.S. degrees from the control and instrumentation engineering from the Seoul National University of Science and Technology (Seoul Tech), Seoul, Korea, in 2001 and 2003, respectively. He is currently working toward the Ph.D. degree in electrical engineering and telecommunications at the University of New South Wales, Sydney, N.S.W., Australia.

He was a Leader of the Seoul Tech student team for the 2003 Future Energy Challenge (FEC). His work at Seoul Tech involved in research on active power

filter, cancel neutral current harmonics in three-phase for-wire systems, UPS and DSP control. His research interests include power conversion technologies in renewable energy system, smart grid, power quality and digital power control.

Mr. Jang is the recipient of the First Place Award from the 2003 FEC Competition, which is sponsored by the U.S. Department of Energy.



Mihai Ciobotaru (S'04–M'08) was born in Galati, Romania. He received the B.Sc. and M.Sc. degrees from the "Dunarea de Jos" University of Galati, Galati, in 2002 and 2003, respectively, and the Ph.D. degree from the Institute of Energy Technology, Aalborg University, Aalborg, Denmark, in February 2009, all in electrical engineering.

From 2003 to 2004, he was a Teaching Assistant with the Department of Electrotechnics, Electrical Machinery and Drives, "Dunarea de Jos" University of Galati. From 2007 to 2010, he was a Postdoctoral Researcher in the Institute of Energy Technology, Aalborg University. In 2010, he joined the Centre for Energy Research and Policy Analysis, The University of New South Wales, Sydney, N.S.W., Australia, where he is currently a Research Fellow. His research activities and interests include development of control strategies for distributed power generation systems, wind turbine and photovoltaic systems, grid-connected power converters, power management of the utility grid using medium-voltage power converters, grid voltage monitoring and synchronization, islanding detection, and grid impedance estimation.



Vassilios G. Agelidis (S'89–M'91–SM'00) was born in Serres, Greece. He received the B.Eng. degree in electrical engineering from the Democritus University of Thrace, Thrace, Greece, in 1988, the M.S. degree in applied science from Concordia University, Montreal, QC, Canada, in 1992, and the Ph.D. degree in electrical engineering from the Curtin University, Perth, WA, Australia, in 1997.

From 1993 to 1999, he was with the School of Electrical and Computer Engineering, Curtin University. In 2000, he joined the University of Glasgow,

Glasgow, U.K., as a Research Manager for the Glasgow-Strathclyde Centre for Economic Renewable Power Delivery. In addition, he has authored/co-authored several journal and conference papers as well as *Power Electronic Control in Electrical Systems* in 2002. From January 2005 to December 2006, he was the inaugural Chair of Power Engineering in the School of Electrical, Energy and Process Engineering, Murdoch University, Perth. From December 2006 to June 2010, he was the Energy Australia Chair of Power Engineering at the University of Sydney. He is currently the Director of the Australian Energy Research Institute, The University of New South Wales, Sydney, N.S.W., Australia.

Dr. Agelidis received the Advanced Research Fellowship from the United Kingdom's Engineering and Physical Sciences Research Council in 2004. He was the Vice President Operations within the IEEE Power Electronics Society for 2006–2007. He was an Associate Editor of the IEEE POWER ELECTRONICS LETTERS from 2003 to 2005, and served as the Power Electronics Society (PELS) Chapter Development Committee Chair from 2003 to 2005. He was an AdCom Member of IEEE PELS for 2007–2009 and the Technical Chair of the 39th IEEE Annual Power Electronics Specialists Conference, Rhodes, Greece.